JOURNAL OF MATERIALS SCIENCE 17 (1982) 126–134

On the various stages of spinodal decomposition in an Al–38 at % Zn alloy

M. VIJAYALAKSHMI, V. SEETHARAMAN, V. S. RAGHUNATHAN
Metallurgy Programme, Reactor Research Centre, Kalpakkam-603102, Tamilnadu, India

Spinodal decomposition of an Al–38 at % Zn alloy in the temperature range 293 to 573 K has been studied by transmission electron microscopy. Microstructural evidences for the existence of various stages of spinodal decomposition, namely, the initial, the corsening and the particulate stages have been established. The morphological characteristics and the different diffusion regimes under which these stages are operative are explained.

1. Introduction

The possibility of spinodal decomposition in Al–Zn alloys was suggested by Munster and Sagel [1] and Graf and Genty [2]. This was confirmed by the classical small-angle scattering experiments of Rundman *et al.* [3] on Al–28 at % Zn. X-ray diffraction studies conducted by Wahi and Anantharaman [4] on the alloys containing 20 and 30 at % Zn revealed the formation of side bands on ageing at temperatures less than 515 K. Electron microscopy results obtained by Ardell *et al.* [5] and Ciach *et al.* [6] show clearly the tweed-like morphology of a spinodally-decomposed product in concentrated alloys. Several attempts have been made to determine the miscibility gap and calculate the spinodal curve [7–9]. Direct evidence to demonstrate the microstructural evolution of the spinodally decomposed products in this system is scarce, though such results have been obtained in other systems such as Cu–Ni–Cr [10]. Therefore, a detailed transmission electron microscopic study of the various stages in the development of the spinodal products in an Al–38 at % Zn alloy has been undertaken and the results of this study are reported in this paper.

2. Experimental procedure

The alloy was prepared by melting accurately-weighed amounts of high-purity aluminium (99.99+%) and zinc (99.99+%). The cast alloy was homogenized at 675 K for a week with intermediate cold working to break up the cast structure. The compositions of the major elements were determined by wet chemical analysis while the impurity contents were analysed by atomic absorption spectroscopy; the results are presented in Table I. The homogenized alloy was cold-rolled into sheets of 0.1 mm thickness for TEM studies. Rectangular pieces were cut from these sheets and ground flat on either side to about 50 μm thickness. The thin samples were then solution-annealed at 675 K for 1 h and quenched immediately into ice water. The sample was quickly transferred to an oil bath for the ageing treatment; the time elapsed between the solution-treatment and the ageing-treatment was kept to a minimum. This heat-treatment was followed by ice-water quenching and electropolishing to obtain samples for electron microscopy. All these precautions were necessary to minimize decomposition at ambient temperature.

TABLE I Impurity contents in the Al–38 at % Zn alloy

Content of each impurity (ppm)				
Cu	Ni	Mg	Si	Fe
4	10	20	20	22

The electropolishing of the samples was carried out by the "window technique" using an electrolyte of 20 vol % perchloric acid and 80 vol % methanol at temperatures below 245 K and a voltage of 20 V. The thin foils were observed using a Philips EM 400 transmission electron microscope.

3. Results and discussion

A tweed-like microstructure characteristic of the spinodally-decomposed product was found to

0022–2461/82/010126–09$02.90/0

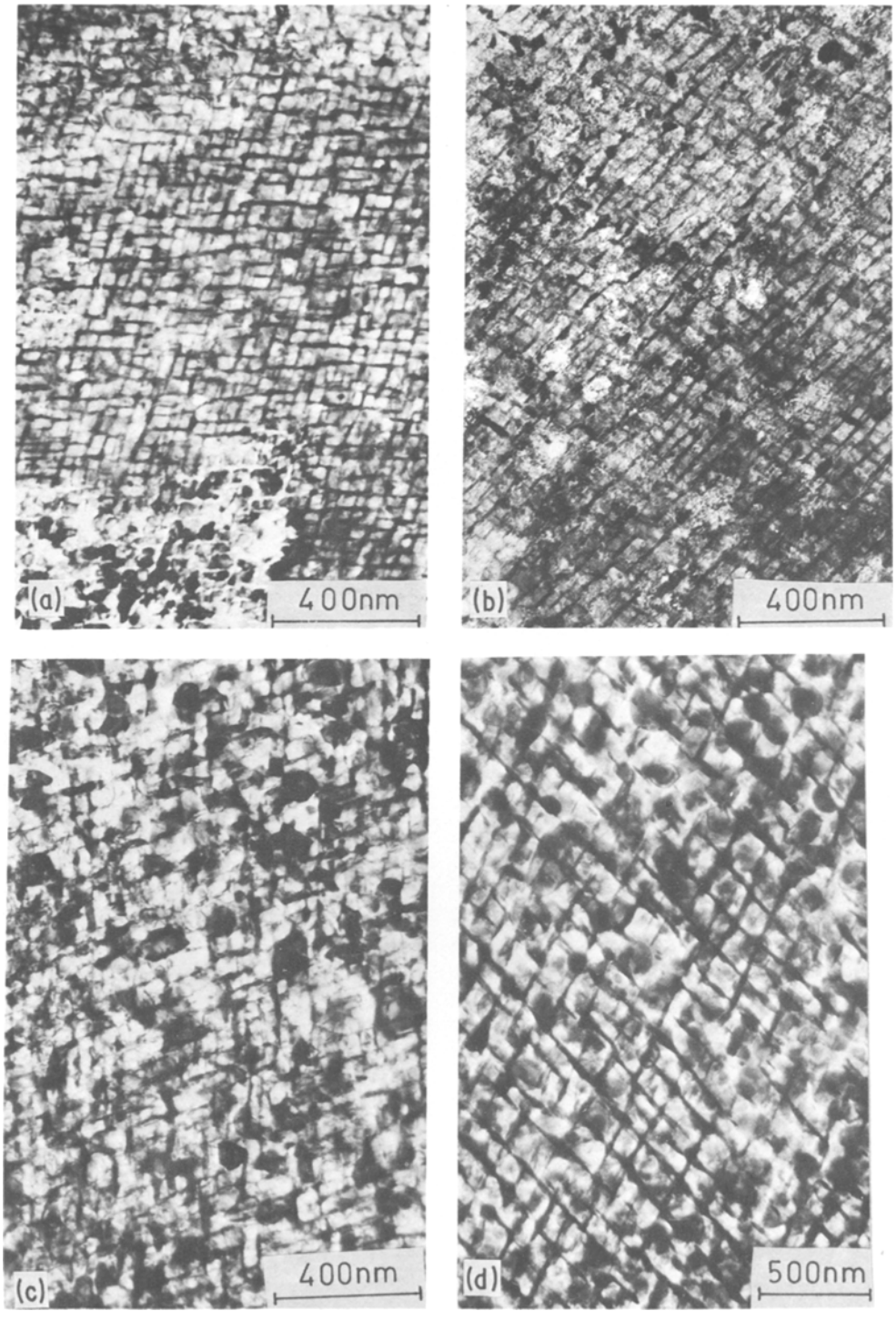

Figure 1 Evolution of the spinodal products on isothermal ageing of solution-treated Al–38 at % Zn at 523 K for various times (a) 15 sec (b) 30 sec (c) 60 sec and (d) 360 sec.

evolve on ageing the high-temperature solid solution, α', at any temperature inside the miscibility gap. Since it has been well established that spinodal decomposition does occur in the Al–Zn system and that the results generally conform to the prediction of Cahn's theory [11] with respect to

the different characteristics of the decomposition, much attention has been focussed on the development of the spinodal products in the present investigation. The evolution with time of the β-Zn phase from an originally unstable α'-phase inside the $\alpha + \beta$ region is found to follow various stages of the decomposition, as illustrated in a series of micrographs in Fig. 1. The decomposition was followed from 15 sec to 10 min at 523 K. As can be seen clearly, the phase mixtures of α-Al and β-Zn exhibit a remarkable degree of interconnectivity with a well-defined composition periodicity, of wavelength, λ, consisting of alternate lamellae of aluminium-rich and zinc-rich regions. It was not possible to perform the "microstructural sequence method" [12] to prove the existence of spinodal decomposition. However, periodicity and alignment along the elastically-soft directions are strong evidences that spinodal decomposition has occurred. These micrographs also exhibit the simultaneous occurrence and growth of equilibrium β-Zn precipitates along the spinodal arms. From the analysis of the selected-area diffraction pattern, it is found that the modulations observed in Fig. 1 are parallel to $\{1\,1\,1\}_\alpha$ planes, the implication of which is discussed below.

The growth rate of the composition modulations will be maximum in the direction that minimizes the elastic modulus, Y. In other words, for cubic alloys the sign of the elastic anisotropy factor, $2C_{44} - C_{11} + C_{12}$, would play a crucial role. The "elastically-soft" directions for crystals having positive anisotropy factor are $\langle 1\,0\,0 \rangle$, while $\langle 1\,1\,1 \rangle$ are the soft directions for crystals associated with negative anisotropy factor. Cahn [11] has further shown that the $\{1\,0\,0\}$ modulations would be associated with a tetragonal distortion of one of the product phases as in the case of Cu–Ni–Fe [13], Cu–Ni–Sn [14] and Cu–Ni–Cr [15, 16], while $\{1\,1\,1\}$ plane waves would lead to a rhombohedral distortion. The present observation that the modulations are along $\{1\,1\,1\}_\alpha$ planes suggests a rhombohedral distortion and a negative anisotropy factor. In fact, Leigh [17] has evaluated the anisotropy factor for an Al–29 at% Zn alloy as -6.4×10^{-4} MN m^{-2}. Thus, it can be seen that the present findings are in conformity with the predictions of Cahn [11].

The wavelength of decomposition can be either measured directly from the enlarged micrographs or by calculation from the spacing of the satellite spots in the diffraction pattern, using the Daniel–Lipson equation [18]. It is well known that the angular separation between the main spot and the satellite spot, $d\theta$, decreases as λ increases and hence, the observation of satellites is possible only if λ is of the order of 4 nm. In the present investigation, the initial values of λ were of the order of 20 to 25 nm and thus it was not possible to detect the presence of satellite spots. Hence, an estimate of the most prominent wavelength of the composition fluctuations was made by measuring the mean distance between the two adjacent α–Al lamellae using bright-field micrographs.

The measured values of λ, corresponding to the maximum growth rate during the various stages of evolution of the decomposition, are shown in Fig. 2. It can be seen that the wavelength remains independent of the ageing time in the initial stages of the decomposition, i.e., until about 30 sec at 525 K, after which the wavelength increases monotonically with an increase in ageing time and reaches a value of about 200 nm within 10 min. The constancy of the wavelength during initial ageing is consistent with the spinodal theory. It may be concluded from Fig. 2 that the value of 25 nm corresponds to λ at 523 K for Al–38 at% Zn. It may also be deduced that the critical wavelength, $\lambda_c = \sqrt{2}\,\lambda = 35$ nm.

3.1. Stages of evolution of spinodal microstructure

The evolution of microstructure of a spinodally decomposing system has been found to consist of

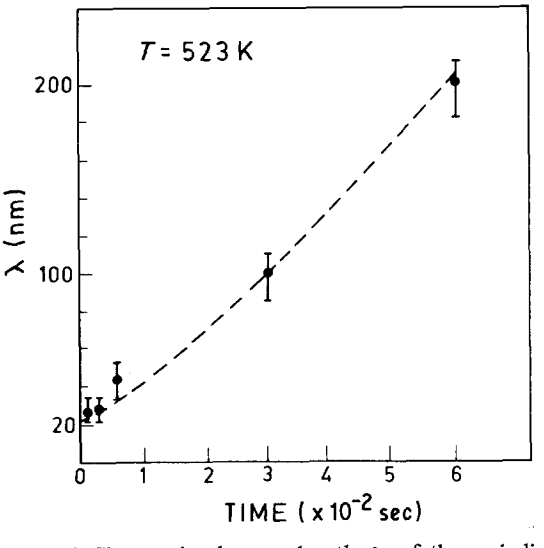

Figure 2 Changes in the wavelength, λ, of the periodic structure on ageing at 523 K.

TABLE II Coarsening stages of the spinodally-decomposed products [10]

Stage	Characteristic feature	λ	Interconnectivity	Particle size
	Spinodal decomposition	Constant	High	Not applicable
I	Coarsening	Increasing	High	Not applicable
II	Degeneration	Constant	Decreasing	Not applicable
III	Particulate coarsening	Not applicable	Not applicable	Increasing
IV	Interface incoherency	Not applicable	Not applicable	Increasing (+ coalescence)

five stages [10], the characteristics of which are presented in Table II. Microstructural evidence for the existence of some of these stages have been obtained in the present study and these are discussed in the following sections.

3.1.1. Spinodal stage

This stage was found to occur in the initial ageing times at all temperatures within the unstable region. The existence of the spinodal stage in the supersaturated α'-matrix at various temperatures is illustrated in Fig. 3. Apart from providing evidence for the existence of the spinodal stage, this series of micrographs also helps the understanding of the dependence of λ on ageing temperature. It is expected from Cahn's theory [11] that there is a decrease in λ as the ageing temperature is lowered, the decrease being very much more pronounced at higher temperatures than at lower temperatures. The composition fluctuations are found to grow along the $\{1\,1\,1\}_\alpha$ planes. At any given temperature, the wavelength is found to remain constant during this stage, consistent with Cahn's theory. A steady build-up of phase contrast in the micrographs during the constant wavelength period, as proposed by Laughlin and Cahn [19], could not be observed owing to the large wavelengths which were set up in the system. During this stage, it was observed that the presence of grain boundaries did not, in any way, influence the decomposition and no preferential nucleation along the grain boundaries was observed.

3.1.2. Coarsening stage

The distinct feature of this stage was found to be the continued existence of the well-interconnected microstructure, which had not given way to a "particulate" structure. The wavelength of the composition fluctuation was no longer constant and the coarsening of the interconnected microstructure was found to obey the $\lambda \propto t^{1/3}$ growth law (see Fig. 4), similar to the diffusion-controlled coarsening of an aggregate of precipitate particles [20, 21]. In spite of the significant coarsening occurring during this stage all the structures showed a remarkably high degree of interconnectivity. Though the degree of interconnectivity is difficult to measure, owing to the absence of any accepted parameter to monitor this variable, it is quite evident from the series of micrographs in Fig. 1 that with a simultaneous increase in the wavelength of the composition fluctuation, the α-Al and β-Zn lamellae of the decomposition products retain a high degree of interconnectivity.

The coarsening stage, Stage I, of the multiply-interconnected phase could occur by three different modes [10]:

(a) The continuous coarsening mode, wherein a continual adjustment of the existing wavelengths results in an increase in its width without destroying the interconnectivity.

(b) The discontinuous coarsening mode, in which the coarsening is initiated by the pre-existing heterogeneities and the coarsened lamellae formed along the grain boundaries proceed further to consume the rest of the matrix containing finer lamellae.

(c) The harmonic coarsening mode, the least probable mechanism, which occurs by the dissolution of some of the existing lamellae and necessarily leads to modulations whose wavelengths are integral multiples of the previous values.

Of the different mechanisms envisaged, the continuous and the discontinuous coarsening modes are found to occur in the Al–Zn system; of these two, continuous coarsening is preferred. The series of micrographs in Fig. 1 illustrates the occurrence of continuous coarsening, on isothermal ageing at 523 K for various times. There is no sign of discontinuous coarsening at any location. In contrast to this, *in situ* hot-stage electron microscopy provided evidence for the occurrence of continuous as well as discontinuous coarsening on cooling the sample from 673 K to 563 and 443 K, respectively. This is illustrated by a series of micrographs in Fig. 5. The discontinuous coarsening

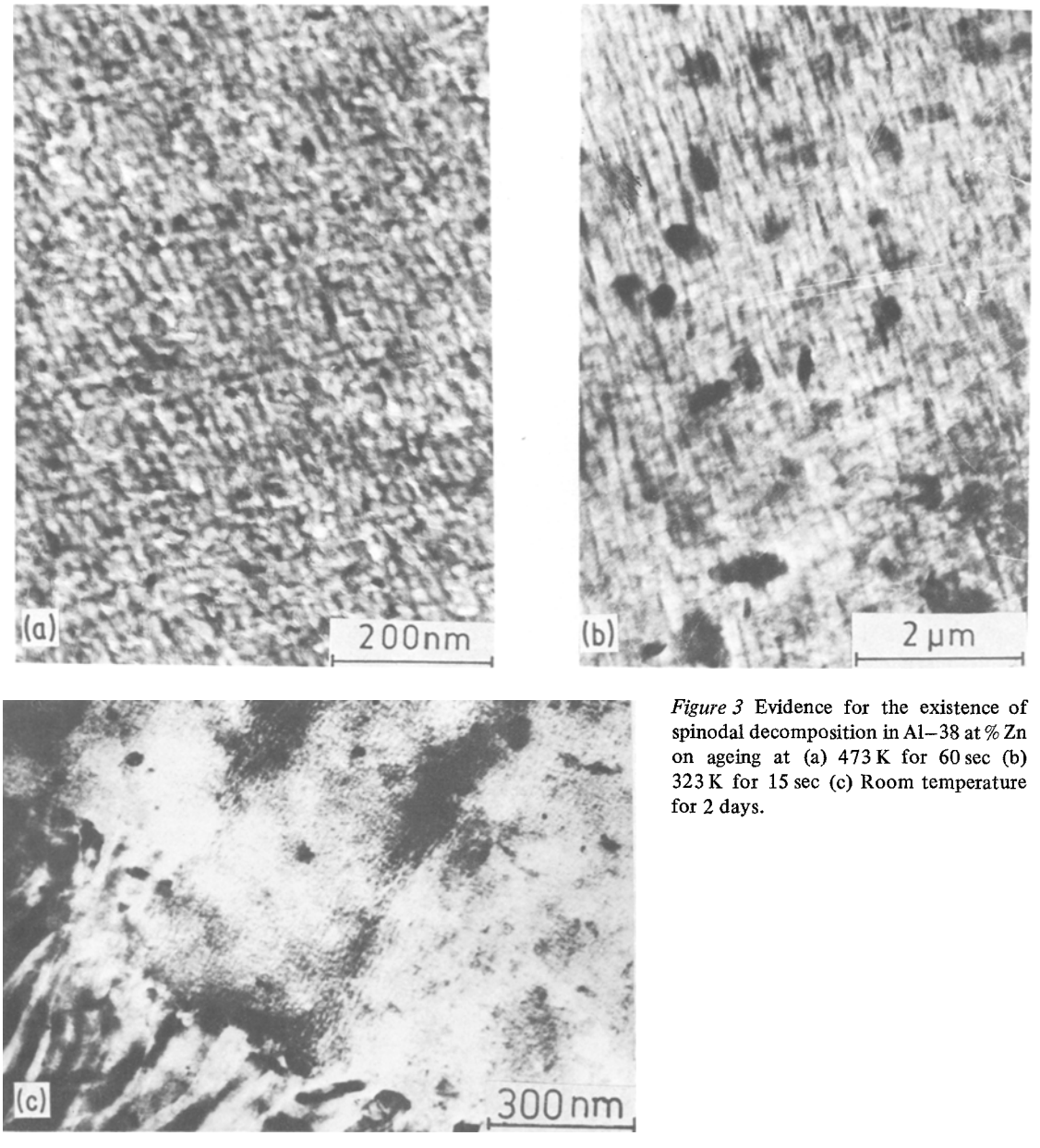

Figure 3 Evidence for the existence of spinodal decomposition in Al–38 at % Zn on ageing at (a) 473 K for 60 sec (b) 323 K for 15 sec (c) Room temperature for 2 days.

mechanism is seen in Fig. 5a on cooling the single phase to 563 K and remaining at this temperature for five minutes. Coarsening by this mechanism requires redistribution of solute atoms along an incoherent interface, between regions of fine and coarse periodicity. Fig. 5b provides an evidence for the continuous coarsening of the initially well-mixed structure on ageing at 443 K. As the structure coarsens, the wavelength increases slowly but continuously followed by the coalescence of the two impinging lamellae. The points marked A, B and C in Fig. 5b are probably such coalescence locations. The existence of such sites indicates the initiation of the break-up of the interconnectivity of the tweed microstructure. On continued ageing at 443 K, the particulate stage, Stage II, sets in, with the spinodal arms losing their interconnectivity, giving rise to an increased density of such coalescence sites and finally transforming into a particulate structure, as shown in Fig. 5c.

3.1.3. Particulate stage

The final break-up of the β-Zn lamellae into discrete particles was found to occur after ageing

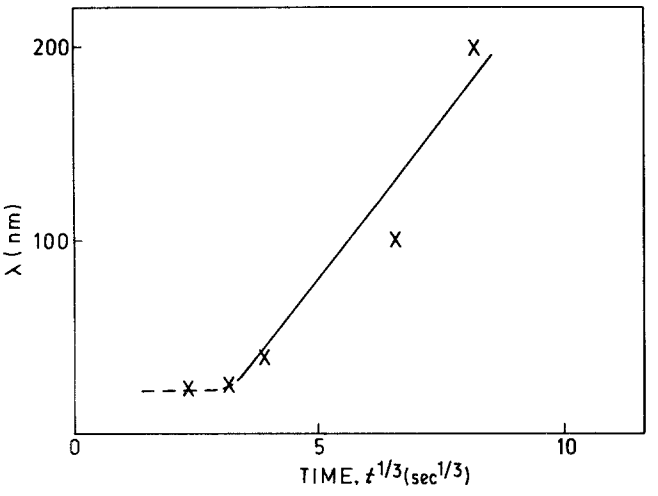

Figure 4 The variation of λ with $t^{1/3}$ at 523 K. The coarsening curve ends where the tweed-like structure changes to a particle morphology.

for ten minutes at 523 K. The degree of interconnectivity changed remarkably; the structure could no longer be described as having a tweed-like morphology, The onset of the particulate Stage II can be clearly seen in Fig. 6. However, Stage III, in which the Ostwald ripening of these particles is expected to take place, could not be observed due to interference from the competing cellular reaction.

3.2. Factors influencing the occurrence of various stages

It is worthwhile noting that the coarsening scheme, as observed in the present work, does not represent the complete picture, as illustrated in Table II, for following reasons: (a) the overlapping of the various stages and (b) interference due to the existence of competing reactions. For example, the formation of equilibrium sheet-like β-Zn precipitates completely replaces the structure developed by spinodal decomposition. Similarily, the rapid kinetics of the cellular reaction, whose advancing interface consumes the spinodally-decomposed matrix, obscures the observation of all the stages.

The formation of equilibrium β-Zn through any one of the processes mentioned above, is evident from the X-ray diffractograms shown in Fig. 7. The most prominent peak of β-Zn, i.e., the $(1\,0\,\bar{1}\,1)_\beta$-peak, makes its appearance even after ageing for one min at 523 K, showing the rapidity of the reaction. It is also noticed that the $(2\,0\,0)_\alpha$-peak is associated with the pronounced asymmetry towards the high angle side. This suggests that, initially, the supersaturated α'-phase decomposes to yield both the α- and α'_m-phases, where α'_m represents Hultgren's extrapolation of the α''(ZnAl)-phase at temperatures below 613 K. As the ageing time is increased, the asymmetry of the $(2\,0\,0)_\alpha$-peak shifts gradually to the low-angle side, indicating that the composition of the matrix slowly approaches that of the equilibrium α-phase. However, long before the reaction $\alpha' \rightarrow \alpha + \alpha'_m$ goes to completion, the competitive reaction, $\alpha' \rightarrow \alpha + \beta(Zn)$, sets in and suppresses the growth of the α'_m-phase.

In general, the continuous reaction process which begins with the spinodal decomposition and ends with the appearance of coarse, discrete, second-phase particles is the result of a series of diffusion-controlled mechanisms. Initially, in the spinodal stage, up-hill diffusion occurs in response to a thermodynamic requirement, leading to a very fine, multiply-connected structure. These interconnected periodic lamellae are then found to coarsen by a gradual increase in wavelength, involving a continuous adjustment in the position of the lamellae during coarsening. The driving force for such coarsening is as follows: owing to the steady build-up in the amplitude of the composition fluctuations at a constant wavelength, the coherency strains across the adjacent lamellae increase, which in turn increase the elastic strain energy associated with the decomposition. This increase in the strain energy demands a decrease in the interfacial surface energy so that the total free energy is minimized. This is achieved by the attainment of a larger but uniform interphase spacing. The main mechanism of diffusion in this stage is essentially by a volume diffusion process, as indicated by the $t^{1/3}$-law. It has been proposed [13] that the diffusion currents which are responsible

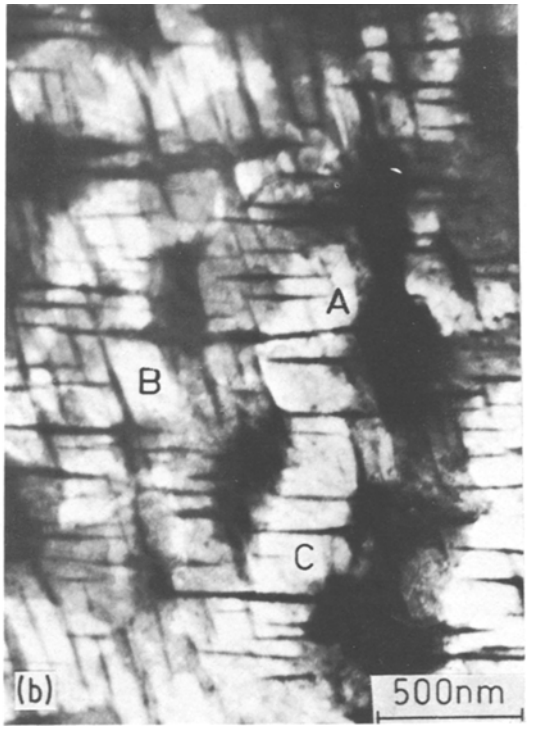

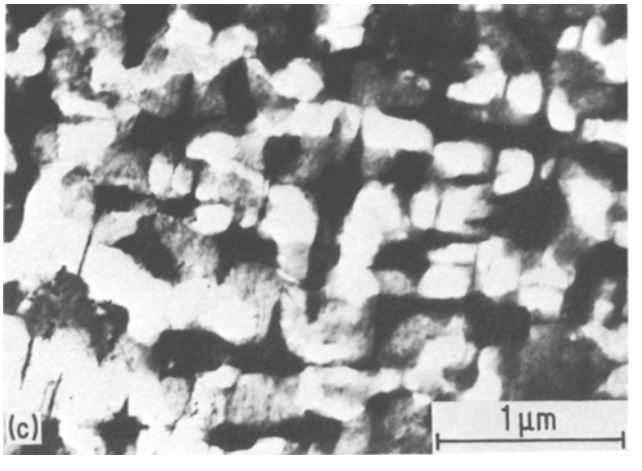

Figure 5 In situ hot-stage electron micrographs illustrating (a) the existence of discontinuous coarsening on cooling from 673 to 563 K; (b) the onset of Stage I coarsening on cooling from 673 to 443 K and holding 443 K for 30 sec (A, B and C are the coalescence points), (c) the formation of discrete β-Zn particles on continued ageing at 443 K for 60 sec (Stage II).

for such a coarsening are influenced by stress fields in the early stages, so that the total energy is minimized for a uniform interphase spacing.

Finally, the attainment of discrete particles involves the break-up of the aligned lamellae at a constant lamellar spacing. The mechanism by which this breaking-up of the interconnected structure occurs is possibly similar to that shown by Cline [22] for the case of parallel rods, in which the instability of the rods to a fluctuation in the rod diameter could lead to the pinching-off of the rods. Instability of such aligned microstructures has also been investigated by other workers [23, 24]. In this case, the operative diffusion mechanism could either be volume or interface controlled; unambiguous determination of the operative mechanism requires a precise knowledge of the kinetics of the change in the aspect ratios of the rod-shaped precipitates. This lot has not been undertaken in the present study and hence the operative diffusion mechanism in this stage could not be identified.

Figure 6 The degeneration from an interconnected "scaffold" structure to a discrete distribution of β-Zn particles on ageing at 523 K for 600 sec.

4. Conclusions

Electron microscopic evidence has been presented to establish the following sequence of the development of spinodally decomposed products in an Al–38 at % Zn alloy.

(a) Spinodal stage: The growth of composition fluctuations with a constant wavelength, the growth being insensitive to the presence of structural inhomogeneities.

(b) Coarsening stage: Two different modes of coarsening have been observed, continuous and discontinuous coarsening. The coarsening of the spinodal wavelength follows a $t^{1/3}$-law retaining the interconnectivity at the same time.

(c) Particulate stage: Coalescence of the interconnected α/β lamellae leads to the breaking-up of the tweed-like morphology and eventually results in the formation of a particulate aggregate in a matrix of α-Al.

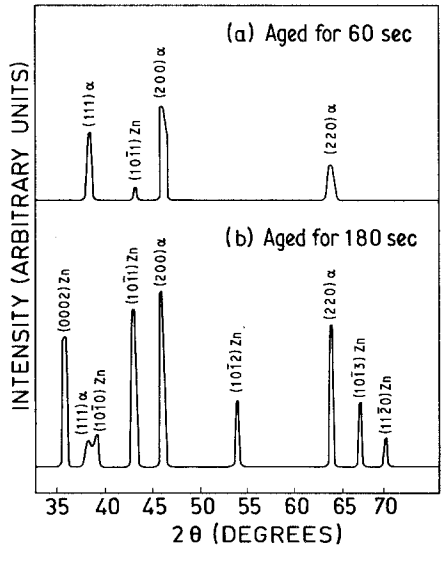

Figure 7 X-ray diffractograms of Al–38 at % Zn alloy aged at 523 K.

Acknowledgements

The authors wish to thank Dr P. Rodriguez, Head, Metallurgy Programme, Reactor Research Centre, for his constant encouragement and advice during the course of this work. They are also grateful to Dr R. Krishnan, Metallurgy Division, BARC, Bombay for many helpful discussions.

References

1. A. MUNSTER and K. SAGEL, *Z. Electrochem.* 59 (1955) 946.
2. R. GRAF and B. GENTY, *C. R. Acad. Sci. (Paris)* 251 (1960) 2517.
3. K. B. RUNDMAN and J. E. HILLIARD, *Acta Metal.* 15 (1967) 1025.
4. R. P. WAHI and T. R. ANANTHARAMAN, *Scripta Metal.* 2 (1968) 681.
5. A. J. ARDELL, K. NUTTAL and R. B. NICHOLSON, "The Mechanism of Phase Transformations in Crystalline Solids" Monograph and Report Series 33 (The Institute of Metals, London 1969).
6. R. CIACH, J. DUKIEWICZ, R. KROGGEL, H. LOFFLER *and* G. WENDROCK, *Krist. Tech.* 10 (1975). 123
7. J. DELAFOND, A. JUNQUA, J. MIMAULT and J. P. RIVIERE, *Acta Metal.* 23 (1975) 405.
8. M. OHTA, T. KANADAM, A. SAKAKIBARA and M. YAMADA, *Phys. Stat. Solidi* A48 (1978) K141.
9. T. R. ANANTHARAMAN and K. G. SATYANARAYANA, *Scripta Metal.* 7 (1973) 189.
10. R. I. SAUNDERSON, P. WILKES and G. W. LORIMER, *Acta Metal.* 26 (1978) 1357.
11. J. W. CAHN, *ibid.* 10 (1962) 179.
12. D. E. LAUGHLIN, *ibid.* 24 (1976) 53.

13. E. P. BUTLER and G. THOMAS, *ibid* **18** (1976) 347.
14. B. G. LEFEVRE, A. T. DANESSA and D. KAILASH, *Metal. Trans.* **9A** (1978) 577.
15. C. K. WU, R. SINCLAIR and G. THOMAS, *ibid.* **9A** (1978) 381.
16. C. K. WU and G. THOMAS, *ibid.* **8A**, (1977) 1911.
17. R. S. LEIGH, *Phil. Mag.* **42** (1951) 876.
18. V. DANIEL and H. LIPSON, *Proc. Roy. Soc.* **A181** (1973) 368.
19. D. E. LAUGHLIN and J. W. CAHN, *Acta Metal.* **23** (1975) 329.
20. I. M. LIFSHITZ and V. V. SLYOZOV, *J. Chem. Phys. Sol.* **19** (1961) 35.
21. C. WAGNER, *Z. Electrochem.* **65** (1961) 81.
22. H. E. CLINE, *Acta Metal.* **19** (1971) 481.
23. M. McLEAN, *Met. Sci.* **12** (1978) 113.
24. RAYLEIGH, *Proc. London Math. Soc.* **10** (1878) 4.

Received 10 June
and accepted 15 June 1981